ACS OMEGA

http://pubs.acs.org/journal/acsodf

Article

Tuning the Ferroelectric Phase Transition of P(VDF-TrFE) through a Simple Approach of Modification by Introducing Double Bonds

Honghong Gong, Xiao Wang, Mengdi Sun, Ying Zhang, Qinglong Ji, and Zhicheng Zhang*

Cite This: *ACS Omega* 2022, 7, 42949−42959

Read Online

ACCESS | Metrics & More | Article Recommendations | Supporting Information

ABSTRACT: Electroactive polymer (EAP) is a kind of intelligent material that, driven by external electric field, could produce changes in shape or volume. As an important class of EAP materials, poly(vinylidene fluoride) (PVDF) based relaxor ferroelectric polymers show remarkable potential for applications in sensors, actuator, and artificial muscles because of their excellent electrostrictive properties. However, the strain of PVDF-based relaxor ferroelectrics relies strongly on a high electric field, which seriously damages their reliability and limits their practical applications as wearable devices. To explore more suitable materials for actuator applications, in this present work, we report the influences of a double bond (DB) on the electroactive properties of P(VDF-TrFE) (TrFE: trifluoroethylene). The crystalline phase of P(VDF-TrFE) is partially destroyed after the DB is introduced, and the molecular chain flexibility of the product P(VDF-TrFE-DB) can be greatly improved. Therefore, P(VDF-TrFE-DB) has a larger electric displacement while having a lower dipole orientation electric field compared with that of P(VDF-TrFE). The result confirms that the DB could tune the ferroelectric properties and effectively reduce the driving electric field of the PVDF-based relaxor ferroelectric polymers. This work offers a strategy for the preparation of novel EAPs with low driving electric fields.

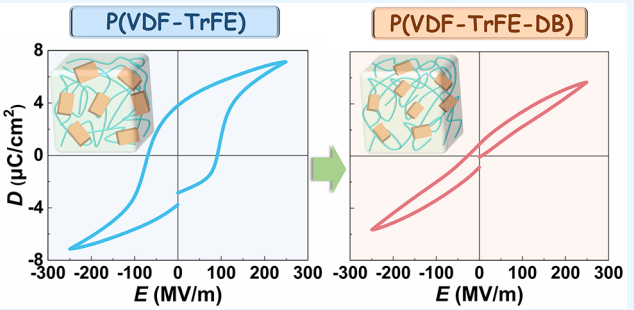

INTRODUCTION

Developing soft actuators like muscles that enable smart, controllable, and robust robot movement is a major challenge in bionic robotics.[1] Smart electroactive polymers (EAPs) are able to change their shape and size under applied electric fields.[2,3] EAPs are widely used in actuators, artificial muscles, sensors, and microreactors and other advanced electromechanical (EM) devices, so they have attracted extensive attention of researchers as a kind of functional material.[4−8] The strain of traditional rigid piezoelectric ceramic EM materials under an electric field is usually less than 0.5%. In contrast, the strain generated by flexible EAPs is about 1 order of magnitude higher.[9−13] In order to make the soft actuators have fast response and high efficiency, efforts have focused on the EAPs represented by dielectric elastomers (DEs),[14−18] electrostrictive polymers,[19] and ferroelectric and relaxor ferroelectric polymers (RFPs)[20−22] recently.

Poly(vinylidene-fluoride) (PVDF) and its copolymers with trifluoroethylene (P(VDF-TrFE)) are the mostly investigated RFPs.[22−28] In P(VDF-TrFE) and beta-PVDF (β-PVDF), the polymer chains are organized in all-*trans* conformation and stacked together to form large scale ferroelectric domains. Under the external electric field, the ferroelectric domains could be polarized and oriented along the direction of electric field.[29−34] During the polarization processes, an electrostrain of 2−3% is observed in P(VDF-TrFE)s as well. Because of the high modules (∼1 GPa) of the copolymers, the electric field induced strain is mainly ascribed to the electrostrictive effects.[23,27] However, the electrostrictive strain in these ferroelectric polymers is not reversible along with the change of the electric field direction because of their inherent polarization hysteresis nature.

The studies on PVDF and its copolymers with TrFE have indicated that these polymers could provide high elastic energy densities and large strain much higher those from traditional piezoceramics.[35] However, this large strain could only be obtained near the breakdown electric field where EM devices are vulnerable and disastrous failure may occur.[36] What is more, it is greatly desirable that practical operation electric fields of EM devices are well below the breakdown field to ensure long-term reliability and safety. That is to say, the high operating electric field seriously limits the applications of RFPs, especially in the field of wearable devices.[1,14] Previous research has shown that the polymer chains could be tailored from long all-*trans* sequences to short ones, thus reducing the size of ferroelectric domains.[37−41] Therefore, the polarization could

Received: August 11, 2022
Accepted: October 31, 2022
Published: November 17, 2022

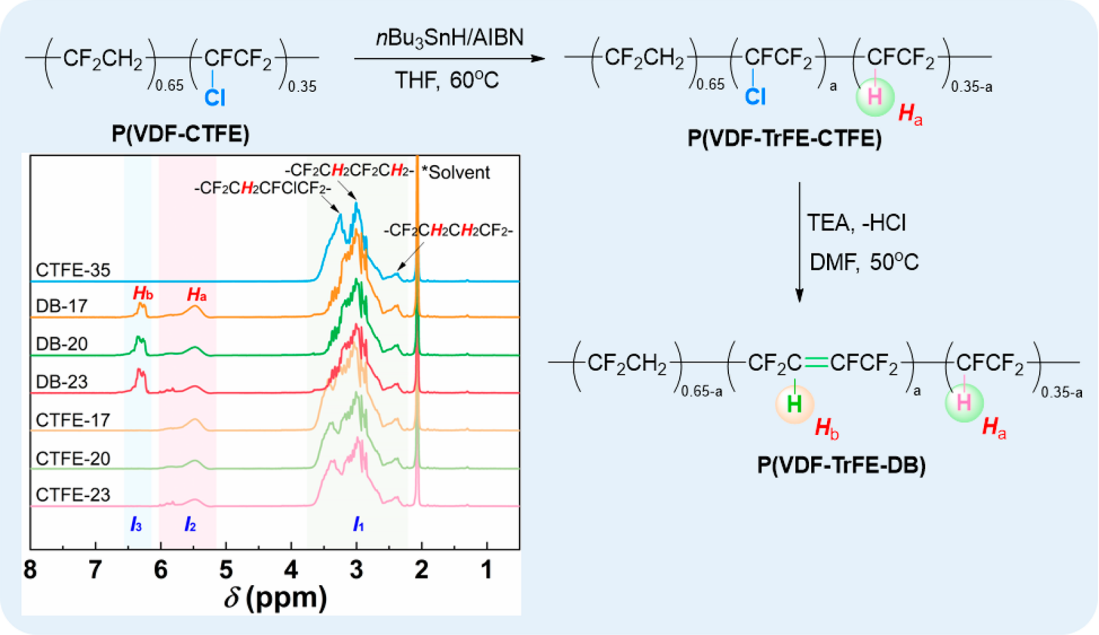

Figure 1. Synthesis of P(VDF-TrFE-CTFE) by the hydrogenation of P(VDF-CTFE) and P(VDF-TrFE-DB) by the elimination reaction of P(VDF-TrFE-CTFE) and ^{1}H NMR spectra of these polymers with different chemical composition.

be easily recovered along with the change of electric field direction. Most importantly, the driving electric field is also reduced accordingly. Due to the contribution of modulus reduction and the transition of normal ferroelectric to RFP, a strain of up to ∼7% was achieved in the relaxor of P(VDF-TrFE-CTFE) (CTFE: chlorotrifluoroethylene) or P(VDF-TrFE-CFE) (CFE: chlorofluoroethylene) at 175 MV/m^{-1}.[42]

Creating an artificial muscle has been one of the grand challenges of science and engineering. Design and preparation of new EAP materials is the key to develop next generation of dielectric elastomer actuators with low driving voltage and large strain for artificial muscle.[1,8,14] Although previous studies have demonstrated that introducing defects, such as bulky monomer units (CTFE, CFE)[43−45] or double bonds (DB),[22,24] into the polymer chain could improve the electrostrictive properties of P(VDF-TrFE), more promising materials are still required to meet the application request. In this work, a succession of P(VDF-TrFE-DB) copolymers with different TrFE/DB compositions is prepared by hydrogenation and then elimination of the P(VDF-CTFE) with a ratio of VDF/CTFE = 65:35 mol %. Instead of bulky CTFE, CF═CH units are employed to serve as a kink to fasten the ferroelectric phase of P(VDF-TrFE). In order to clarify the influence of ferroelectric phase transition after introducing DBs into the molecular chain on the dielectric and electromechanical performances of P(VDF-TrFE) films, a systematic research of the crystalline, dielectric, ferroelectric, and electromechanical properties of these polymer films has been conducted. This work provides a promising strategy for the design and preparation of EAPs based on RFP with excellent electromechanical performances.

EXPERIMENTAL SECTION

Materials. P(VDF-CTFE) (VDF/CTFE = 65:35 mol %, M_w = 130,000, polydispersity index ($Đ$) = 2.20) was obtained from Zhonghao Chenguang Research Institute of Chemical Industry (Chengdu, China). Tetrahydrofuran (THF) was dried and distilled from sodium/benzophenone under nitrogen, and azobis(isobutyronitrile) (AIBN) was recrystallized from ethanol before use. Tri(*n*-butyl)tin hydride (nBu$_3$SnH, Aldrich, 99.99%), *N*,*N*-dimethylformamide (DMF), triethylamine (TEA), and the other chemicals were used directly without any treatment.

Instruments and Characterization. Nuclear magnetic resonance (^{1}H NMR) spectra were recorded on a Bruker spectrometer (400 MHz, Advance III) used acetone-d_6 as solvent. Differential scanning calorimetry (DSC) was carried out on a DSC 200 PC analyzer (Netzsch, Germany) in N_2 atmosphere at a scanning rate of 10 °C min^{-1}. Fourier transform infrared (FTIR) spectroscopy of the films was obtained on a Tensor 27 (Bruker, Germany) with a resolution of 1−0.4 cm^{-1} in transmission mode. X-ray diffraction (XRD) analysis was conducted on a Rigaku D/MAX-2400 diffractometer (Rigaku Industrial Corp., Japan). The wavelength of the X-ray was 1.543 Å (Cu $K\alpha$ radiation, 40 kV, and 100 mA), and the scanning rate was 4° min^{-1}.

Gold electrodes (thickness 50−80 nm) were sputtered on both surfaces of the polymer films with a JEOL JFC-1600 autofine coater (Japan) in order to characterize the electric properties. The dielectric properties were measured at a frequency ranging from 100 Hz to 1 MHz at 1 V using Novocontrol Technologies, concept 80. The displacement−electric field (D−E) hysteresis loops at room temperature were determined on a Premiere II ferroelectric tester from Radiant Technologies, Inc., where AC electric fields with an increment of 25 MV m^{-1} were applied onto polymer films with a triangular waveform at a frequency of 10 Hz and 50 MV m^{-1} with a square waveform. The thickness of the polymer films under the electric field is tested by MTI-2100 equipped with a laser probe of 2032R.

Synthesis and Characterization of P(VDF-TrFE-DB) Polymer. The hydrogenation of P(VDF-CTFE) was conducted following the procedure as our previous work[46] and shown in Figure 1. P(VDF-CTFE)(65:35 mol %) (10.0 g) and

https://doi.org/10.1021/acsomega.2c05172
ACS Omega 2022, 7, 42949−42959

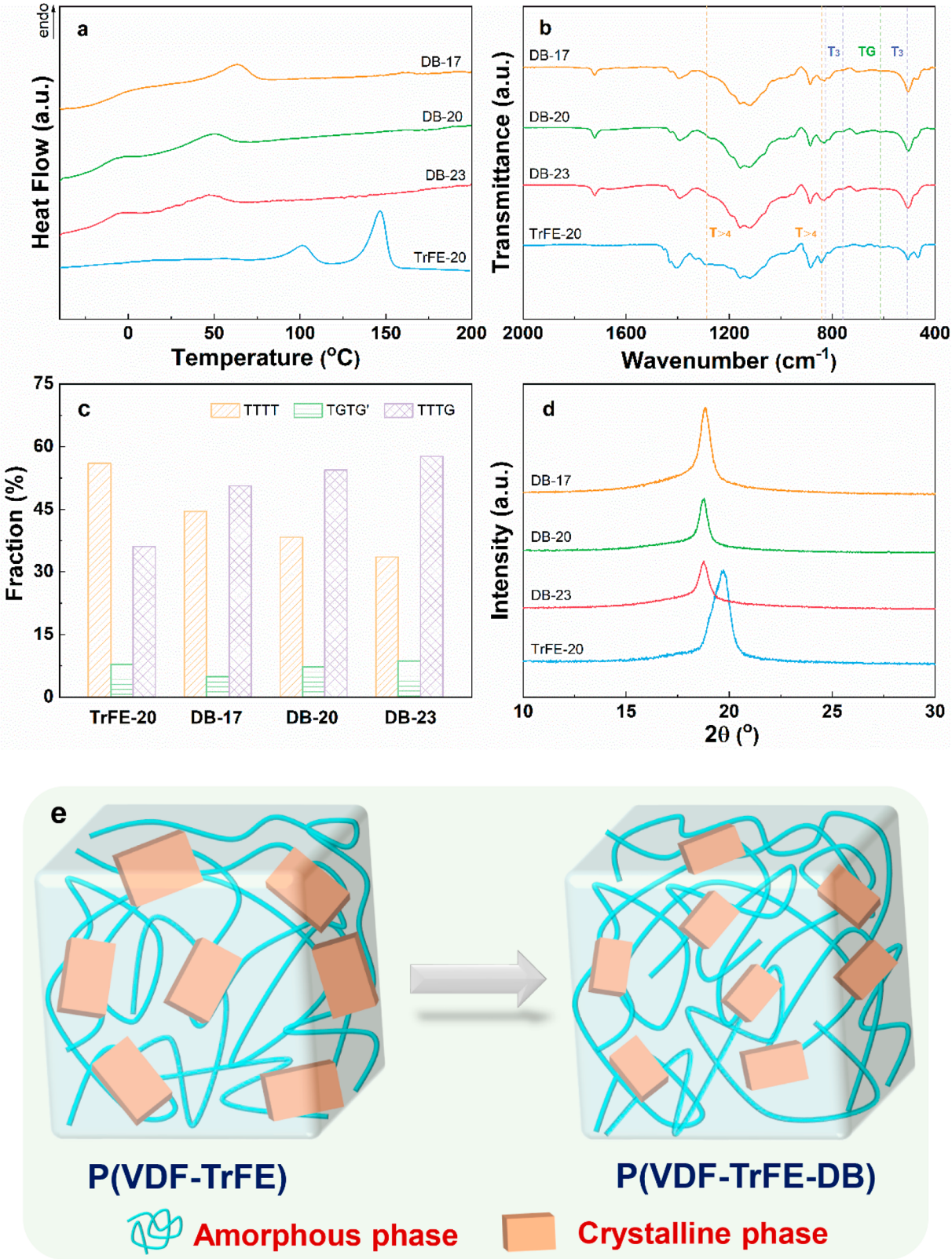

Figure 2. Crystallization and phase transition characterization of polymers. (a) DSC curves, (b) FTIR spectra, (c) fraction of different chain conformations, (d) XRD patterns of P(VDF-TrFE) and P(VDF-TrFE-DB)s polymers, and (e) schematic diagram of the change of the crystalline phase after the introduction of DBs.

AIBN (0.350 g, 2.13 mmol) were added into a 500 mL Schleck flask, and the flask was injected with dry THF (300 mL) after three cycles of vacuum pumping−nitrogen supply. After all P(VDF-CTFE) was dissolved into a homogeneous solution; 20.1 mmol of nBu$_3$SnH (5.41 mL) was injected using syringe. The reaction proceeded at 60 °C for 24 h, and then the reaction solution was quenched with methanol, and precipitated in a mixture of methanol and water with a volume

https://doi.org/10.1021/acsomega.2c05172
ACS Omega 2022, 7, 42949−42959

ratio of 1:1. Then the precipitant was rinsed several times with *n*-hexane. The crude product was dissolved in acetone and precipitated in methanol/water mixture for three times. The white solid product was obtained after the precipitate was dried under reduced pressure at 40 °C. The procedure was repeated with different amounts of nBu$_3$SnH and AIBN to obtain products with different TrFE/CTFE content.

P(VDF-TrFE-DB) was obtained by the elimination reaction of P(VDF-TrFE-CTFE) using the following procedure as descried in our previous work[24] and also shown in Figure 1. Into a 100 mL round-bottom flask equipped with magnetic stirrer, the required amount of TEA was added after P(VDF-TrFE-CTFE) (2.0 g) was completely dissolved in 60 mL of DMF. The reaction solution was powerfully stirred at 50 °C for 24 h, and then the mixture was precipitated in a 5 vol % HCl solution in order to remove the residual TEA. The precipitant was dissolved in acetone and precipitated in methanol for three times before it was dried at 50 °C under reduced pressure. The chemical composition of the resultant polymer was determine by ^{1}H NMR spectrum and could be estimated from the calculation results. For the convenience of subsequent discussion, the samples were named as follows according to the content of CTFE or DB, the pristine P(VDF-CTFE)(65:35 mol %) was named as "CTFE-35", the products P(VDF-TrFE-DB)(65:18:17 mol %), P(VDF-TrFE-DB)(65:15:20 mol %), and P(VDF-TrFE-DB)(65:12:23 mol %) are named as "DB-17", "DB-20", and "DB-23", respectively.

Fabrication of Polymer Films. The copolymer films were prepared by casting the solution (about 25 mg/mL in DMF) onto the glass plates with polytetrafluoroethylene coating. The glass plates with the films were kept at 180 °C for 4 h followed by immediate quenching in an ice−water bath (0 °C) after the solvent was evaporated completely at 70 °C. The films were peeled off from the glass plates for subsequent characterizations.

RESULTS AND DISCUSSION

Crystallization and Ferroelectric-Paraelectric (F−P) Phase Transition of P(VDF-TrFE-DB). The crystalline property and ferroelectric phase transition of the ice−water quenched sample films were examined using DSC, FTIR, and XRD methods. As shown in Figure 2a, Figure S1, and Table S1, only one glass transition temperature (T_g) and no melting peak were observed in CTFE-35 since the bulky Cl atoms hindered the formation of the lattice structure of polymer chain. As shown in Figure S1, the institution of CTFE with TrFE leads to the crystallization and the formation of ferroelectric phase at the same time, which can be identified by the new endothermic peaks at 52.4, 53.6, and 78.4 °C in P(VDF-TrFE-CTFE)s. It has been well reported that the crystalline and ferroelectric phases are generated by the all-trans conformation of VDF-TrFE sequence, and CTFE is serving as bulky defect to tailor the size and content of crystalline and ferroelectric grains.[25] Interestingly, after elimination, the displacement of CTFE by DB results into slightly improved crystalline and ferroelectric performance. As shown in Figure 2a, Figure S2 and Table S1, the crystallinity of DB containing copolymers are larger than that of pristine P(VDF-TrFE-CTFE) and the relevant melting temperature is reversed. That means DB may play the similar role as that of CTFE in tailoring the ferroelectric and crystalline phase of P(VDF-TrFE).

The T_g, melting point (T_m), and crystallinity (X) of P(VDF-TrFE-DB)s polymers all decreased with the increase of DB units, from −12.1 to −19.8 °C of T_g, 63.3 to 49.3 °C of T_m, and 7.09% to 5.35% of X, respectively. It was well-known that DB can favor the spinning of the adjacent C−C single bond, which may increase the flexibility of the polymer molecular chain and reduce the T_g. On the other hand, the DB is serving as a defect as CTFE to the crystalline phase. The more defects that were incorporated, the shorter was the molecular chain that folded into the crystalline phase, and the thinner were the crystals that formed, and so the X and T_m decreased for P(VDF-TrFE-DB)s polymers with the same VDF and TrFE units but different DB content. Comparing with that of the P(VDF-TrFE) 80/20 whose results are listed in Table S1, both X and T_m of DB copolymers (ca., DB-20) are significantly lower. X and T_m of DB-20 are 6.23% and 53.6 °C, while X and T_m of TrFE-20 are 15.67% and 142.6 °C, respectively. These results could further confirm the defect effect of DB on the formation of crystalline and ferroelectric phase of P(VDF-TrFE).

FTIR and XRD were measured and shown in Figure 2 panels b−d, in order to further study the crystalline phase structure of the polymers. In P(VDF-TrFE-DB)s polymers, a new absorption peak appeared near 1720 cm^{-1}, which came from the stretching vibration of the DB introduced in the polymer. The polymer chain in TrFE-20 films possesses a conspicuous TTTT ($T_{>4}$) sequence characterized with the remarkable bands at 840 and 1280 cm^{-1}, the invisible TTTG (T_3) sequence absorption at 512, 776, 812 cm^{-1}, and the TGTG′ (TG) sequence absorption at 532, 614, 764, 855, 976 cm^{-1}.[23,24] But P(VDF-TrFE-DB) has a very small absorption peak related to TTTG conformation, and the intensity of the absorption peak related to TTTT conformation decreases. This illustrates that the DB will reduce the long-range all-trans conformation and increase the short-range TTT conformation.

The fractions of TTTT, TTTG, and TGTG′ conformation of the P(VDF-TrFE) and P(VDF-TrFE-DB) are calculated from FTIR spectra as shown in the previous work,[22,24] and the results are displayed in Figure 2c to further analyze the chain conformation. With the increase of DB content, the TTTT conformation in P(VDF-TrFE-DB) decreases (47% in DB-17, 39% in DB-20, and 35% in DB-23), while the conformation of TTTG and TGTG′ increases. It is known that introducing a DB into P (VDF-TrFE) is equivalent to introducing a defect of TG conformation in the long-range ordered TTTT conformation, destroying the strong coupling between molecular chains. As mentioned above concerning DSC analysis, the DBs in the polymer are more likely to enter the crystal lattice and effectively act as "defects" in the conformation, changing the long-range order of molecular chains into short-range order. This does not destroy the weak coupling effect while it weakens the strong coupling effect, which is conducive to the appearance of the relaxed ferroelectric phase.

When comparing polymers of TrFE-20 and DB-20 with the same VDF and TrFE content, it is found that in TrFE-20, the percentage of TTTT conformation is about 58%, while the TTTG conformation is only about 34%, and the TG conformation is about 8%. In DB-20, the percentage of TTTT conformation is reduced to about 38%, while the TTTG conformation is increased to about 55%, and the TG conformation is also 7%. That illustrates that DBs will introduce the G conformation, cutting the long-range all-*trans* conformation, thereby reducing the content of the TTTT

https://doi.org/10.1021/acsomega.2c05172
ACS Omega 2022, 7, 42949−42959

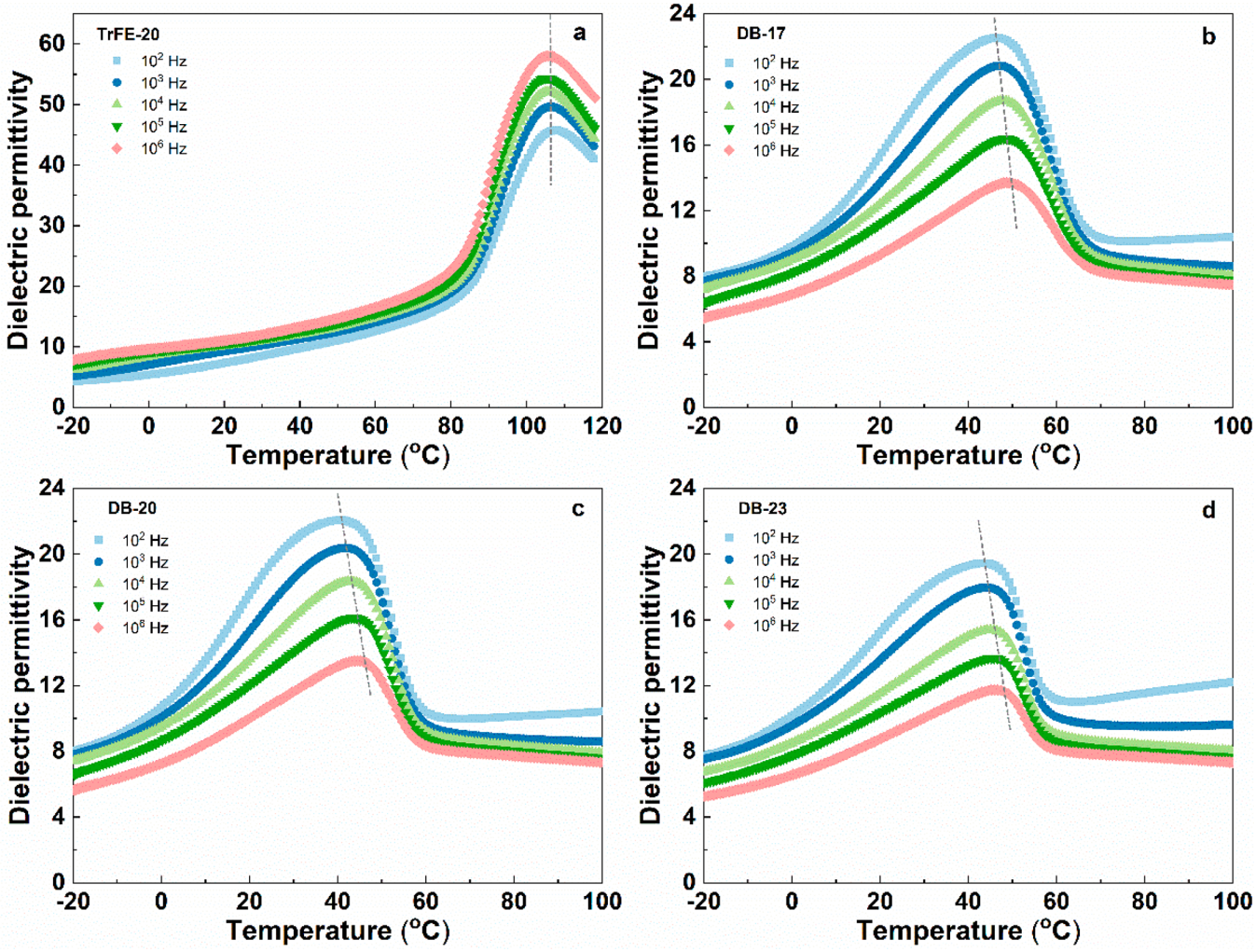

Figure 3. Dielectric permittivity dependence on the temperature of (a) P(VDF-TrFE) (TrFE-20) and (b, c, d) P(VDF-TrFE-DB)s [(b) DB-17, (c) DB-20, (d) DB-23] polymers.

conformation, forming more TTTG conformations, and helping to obtain the relaxor ferroelectric phase.

Figure 2d shows the XRD spectra of P(VDF-TrFE) and P(VDF-TrFE-DB)s polymers, and all polymers have only one single diffraction peak. When the content of DBs increases, the 2θ value of the diffraction peak in P(VDF-TrFE-DB)s decreases, which means the interplanar spacing increases and the grain size becomes smaller (the result shown in Table S2). As mentioned above, DBs can bring more G conformations, and as a result, the molecular chain spacing becomes larger. With the increase of DBs, the defects in the crystal phase increase; thus, the thickness of the wafer decreases, and the crystallinity decreases (Figure 2e).

Comparing TrFE-20 with DB-20, both XRD patterns exhibit only one diffraction peak, but their strength and position are different. First, the diffraction peak of TrFE-20 is stronger than that of DB-20, which means the introduction of DBs will reduce the crystallinity, agreeing well with DSC analysis results. Second, TrFE-20 has the smaller wafer thickness (14.30 nm) than that of DB-20 (16.23 nm). Finally, the TrFE-20 diffraction peak is located at 19.70°, while that of DB-20 is lower, at 18.76°. That is because the diffraction peak in P(VDF-TrFE) comes from the (110)/(200) crystal plane in the ferroelectric phase, while that of DB-20 comes from the (110)/(200) crystal plane in the paraelectric phase. In addition, the molecular chain spacing of TrFE-20 is 4.50 Å, which is smaller than 4.70 Å of DB-20 (Table S2). From the above FTIR analysis results, after the introduction of DBs, the G conformation forms in the long-range ordered TTTT conformation. That will increase the molecular chain spacing, weaken the strong coupling between molecular chains, and transform the ferroelectric phase copolymer into the relaxation ferroelectric phase.

Dielectric Properties under Low Electric Field. Temperature-dependent dielectric spectroscopy is used to characterize the phase transition of P(VDF-TrFE) and P(VDF-TrFE-DB)s to investigate the dielectric properties of polymers under a low electric field (1 V bias). And the result was shown in Figure 3 and Figure S3. There is a very narrow peak near 110 °C in TrFE-20 (Figure 3a). This peak does not show temperature dependence and comes from the ferroelectric phase transition. However, as the temperature increases, all P(VDF-TrFE-DB)s polymers exhibit the Curie transition peaks, but the position and shape of the peaks are different (Figure 3b–d). These temperature-dependent and broad peaks are the phase transition peaks of the relaxation ferroelectric phase, which is consistent with the previous discussion that P(VDF-TrFE-DB)s polymers are relaxor ferroelectrics.

https://doi.org/10.1021/acsomega.2c05172
ACS Omega 2022, 7, 42949−42959

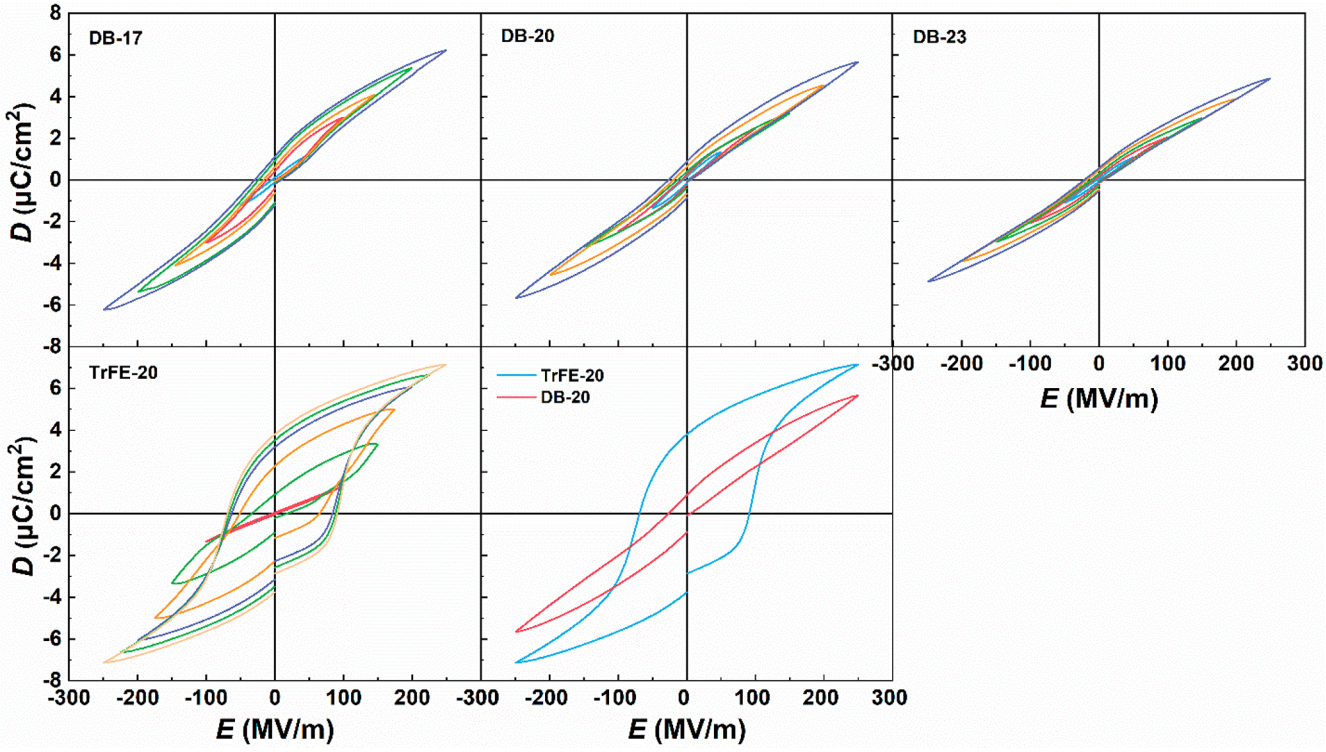

Figure 4. *D*−*E* loops of P(VDF-TrFE) and P(VDF-TrFE-DB)s polymers.

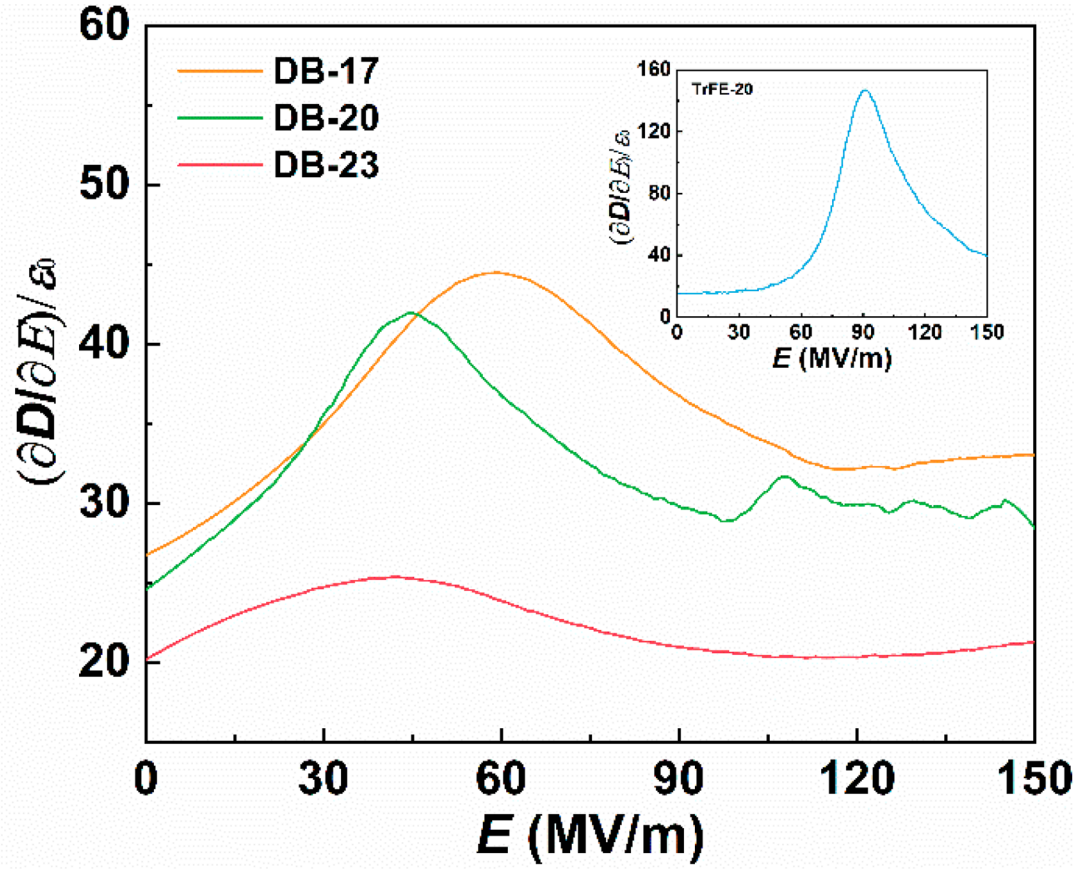

Figure 5. $(\partial D/\partial E)/\varepsilon_0$ of P(VDF-TrFE-DB)s and P(VDF-TrFE) (inset) polymers.

After the introduction of DBs, the Curie transition temperature (T_C) decreases from 110 °C to about 50 °C, and the maximum dielectric constant also drops from about 60 to 20. The G conformation increases the molecular chain

https://doi.org/10.1021/acsomega.2c05172
ACS Omega 2022, 7, 42949−42959

spacing, weakening the coupling between molecular chains, so the dipole in the ferroelectric domain can be transformed into the paraelectric phase at a lower temperature, and the T_C is reduced. The introduction of DB could bring about the TTTG conformation and cause the crystallinity, and the content of the ferroelectric phase and relaxor ferroelectric phase is significantly decreased. That is responsible for the decrease of both the T_C (from 49.6 to 45.3 °C, at 10^6 Hz) and the maximum dielectric constant (from 22 to 18) with the increase of the DB content.

Dielectric Properties under High Electric Field. The dielectric behavior of polymers under high electric fields is examined by the $D-E$ hysteresis loops at 10 Hz, and the results are presented in Figure 4. The $D-E$ loops of P(VDF-TrFE-DB) are rather thin, and both the coercive electric field (E_c) and the remnant polarization value (P_r) are very low. This is very different from the typical ferroelectric phase. Under an electric field less than 50 MV/m, the loops are approximately linear because there are only very few dipoles from small ferroelectric domains and the amorphous phase may be oriented. When the electric field is increased to 100 MV/m, the loop hysteresis appears, indicating that the dipoles in the ferroelectric domains start to orient in large amounts, and the rather low content of ferroelectric domains in the polymer thanks to the defect effect of double bonds is revealed. As mentioned above, the TTTT conformation decreases and the TTTG conformation increases when the content of DBs increases, and the ferroelectric domains are more easily oriented and recovered. Therefore, E_c decreases from −23.1 MV/m of DB-17 to −19.7 MV/m of DB-20 and −18.6 MV/m of DB-23. As compared to the rectangular $D-E$ loops of P(VDF-TrFE) in the normal ferroelectric phase, DBs turn the P(VDF-TrFE-DB)s into relaxor ferroelectrics characterized with narrowed loops and rather small P_r.

The relative dielectric constant ($(\partial D/\partial E)/\varepsilon_0$) of P(VDF-TrFE-DB)s and P(VDF-TrFE) is calculated from $D-E$ loops to study the dependence of dielectric behavior on the electric field, and the result is illustrated in Figure 5. The electric field corresponding to the maximum dielectric constant is E_m, and the value is related to the polarization capability of dipoles. When E_m is reached, most dipoles are oriented. If the coupling of the molecular chains in the ferroelectric domain is strong, a higher electric field is required to orient the dipoles, thus a large E_m will be observed.

It is seen from Figure 5 that the E_m could be detected under a certain electric field for all the samples. For P(VDF-TrFE-DB) polymers, E_m is decreased from 59 MV/m to around 41 MV/m when the content of DBs increases. The introduction of more DBs as defects could continuously reduce the size of the ferroelectric domains and weaken the interaction between molecular chains. Therefore, the transition from normal ferroelectric of TrFE-20 to the relaxor ferroelectric phase of P(VDF-TrFE-DB)s copolymers is responsible for the reduced E_m. The reduced E_m in P(VDF-TrFE-DB)s suggests that the ferroelectric domain is more easily polarized and the dipole orientation is easier.

Ferroelectric Property of the Polymers. The ferroelectric performance could be further evaluated by the remnant polarization (P_r), maximum polarization (P_m), and leakage conduction polarization (P_c) of the polymers as displayed in Figure 6, where all the films were polarized under a square-wave electric field at 200 MV/m for 0.1 s.[47] For P(VDF-TrFE-DB)s, P_m decreases from 5.0 μC/cm^2 to 4.0 μC/cm^2 with

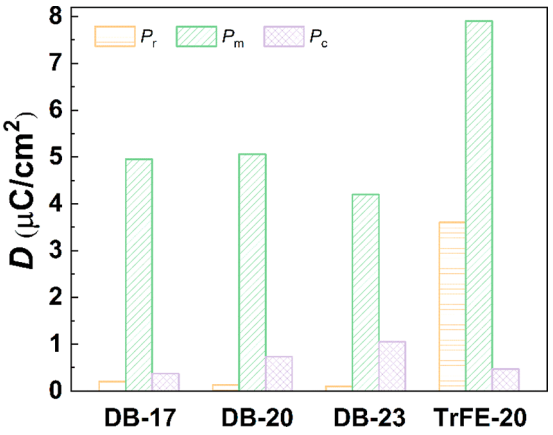

Figure 6. P_r, P_m, and P_c of P(VDF-TrFE-DB)s and P(VDF-TrFE) polymers.

increasing DB content. The P_m values of DB-17 and DB-20 are rather close because they have similar crystallinity. As the crystallinity reduces, the ferroelectric domains of the polymer and the P_m value decrease and the leakage conductance increases. That may address the increased P_c from 0.4 μC/cm^2 to 1.1 μC/cm^2 from DB-17 to DB-20.

P_m value of TrFE-20 is detected as 7.9 μC/cm^2 under the same condition, while its P_r is as high as 3.9 μC/cm^2, and the P_c is only 0.5 μC/cm^2. But for DB-20, its P_m is 5.0 μC/cm^2 while its P_r does not exceed 0.3 μC/cm^2. That is ascribed to the reduction of crystallinity induced by the introduction of DB, resulting in a decrease in ferroelectric domains size and P_m. Meanwhile, the reduced size of ferroelectric domains in DB-20 allows them to be polarized and depolarized quickly along with the flipping of the electric field. As a result, the remnant polarization is mostly eliminated.

Electrostrictive Performances of the Polymers. Apart from piezoelectricity, the introduction of DB also has a great impact on the electrostrictive performances as well because of the crystalline change and ferroelectric phase transitions. For PVDF-based ferroelectric polymers, the electrostriction strain under the electric field is usually correlated to the change of chain conformation and transition of the ferroelectric phase, which could be calculated by the equation of $S = QP^2$, Q refers to the electromechanical coupling coefficient, which is characterized by the energy transfer efficiency during the processes of charging and discharging. The relationship between strain and electric field is measured on an MTI-2100 Fotonic sensor equipped with a laser probe of 2032R, where the electric field is consistent with $D-E$ loops. As shown in Figure 7(a,b), the strain curve of TrFE-20 presents the standard butterfly-like shape of a ferroelectric, which is mainly derived from the electrostriction of the ferroelectric phase. However, the strain curve of DB-20 is finer and shows a relaxor ferroelectric profile. The main source and composition of strain and the influence of Maxwell stress on strain magnitude will be analyzed in detail in the following section.

The maximum strain of P(VDF-TrFE-DB)s and P(VDF-TrFE) is picked to compare the strain obtained under the varying electric field. As shown in Figure 7(c), the strain of P(VDF-TrFE-DB)s slowly increases when the electric field is below 50 MV/m. And the strain increases rapidly once the electric field is over 50 MV/m. In addition, the electric field of strain sharply decreases from 60 MV/m to 40 MV/m with the increase of DB content. The small strain under the low electric

https://doi.org/10.1021/acsomega.2c05172
ACS Omega 2022, 7, 42949−42959

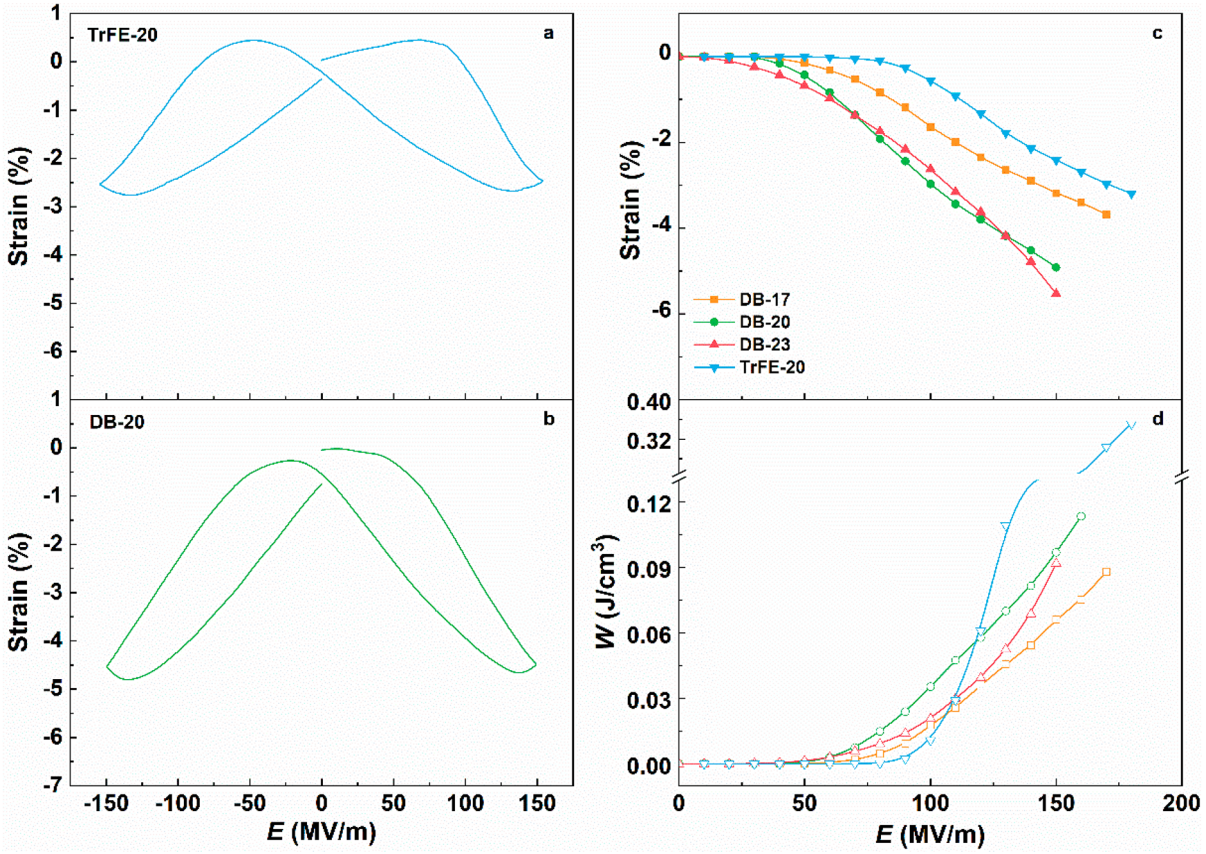

Figure 7. Strain vs electric field curves of (a) TrFE-20 and (b) DB-20; (c) strain (S_3) of TrFE-20 and P(VDF-TrFE-DB)s films as a function of the electric field at 10 Hz; (d) volumetric elastic energy density of TrFE-20 and P(VDF-TrFE-DB)s under the applied electric field at 10 Hz.

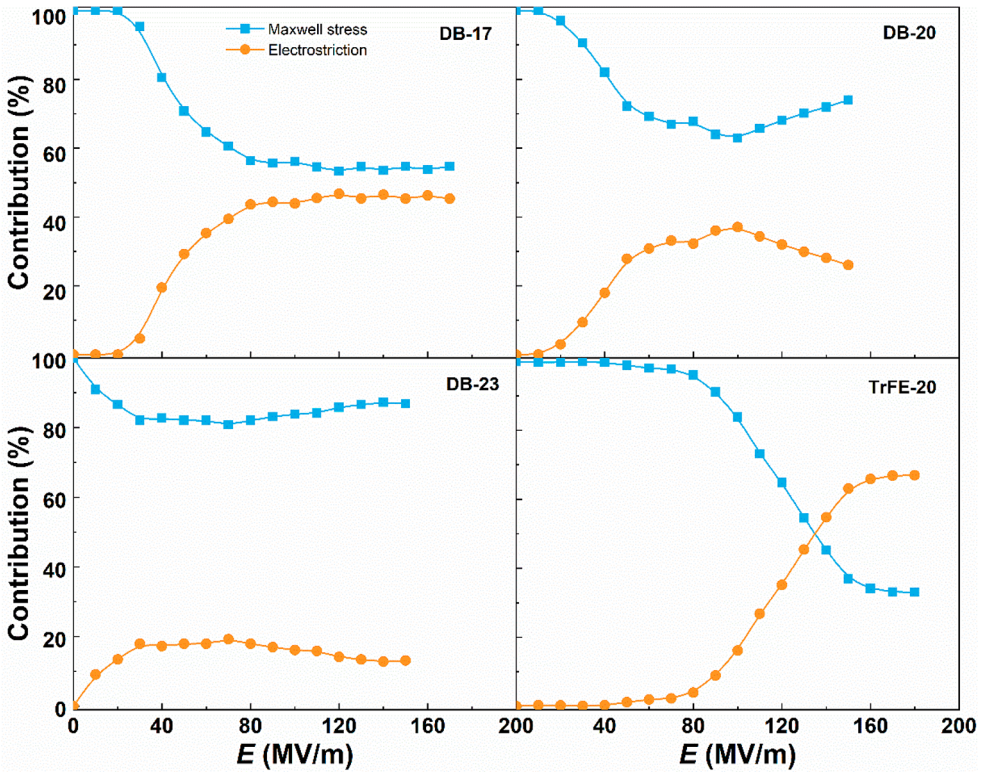

Figure 8. Maxwell stress and electrostriction effects of the percentage of contribution of P(VDF-TrFE-DB)s and P(VDF-TrFE), calculated by $S_M/S_3 \times 100$ and $S_E/S_3 \times 100$.

https://doi.org/10.1021/acsomega.2c05172
ACS Omega 2022, 7, 42949−42959

field occurs because there are a few dipoles under the low electric field. As the content of DBs increases, the distance between molecular chains in the polymers becomes larger, and the ferroelectric domains size reduces, the dipoles can be oriented, and large strains appear under the lower electric field.

In contrast, the strain of TrFE-20 starts to increase suddenly at 90 MV/m electric field, which is about 50 MV/m larger than that of DB-20. The strain of TrFE-20 increases quickly from 90 to 150 MV/m, and the speed of change becomes slower when the electric field is over 150 MV/m. That suggests the major strain of TrFE-20 is associated with the polarizing and saturation of ferroelectric grains. However, the strain of DB-20 under a high electric field (E > 50 MV/m) is increasing continuously, which indicates the strain is more than the polarization of ferroelectric grains, and it will be analyzed in detail below.

The volumetric elastic energy density (W) of the actuator materials driven by the electric field, an important property to measure its electromechanical transformation ability, can be calculated by eq 1:

$$W = \frac{YS_3^2}{2} \tag{1}$$

where Y and S_3 are Young's modulus and the strain, respectively. By taking Y and different S_3 varied with E into above equation, the curve of W *vs* E is obtained as shown in Figure 7(d). As suggested by eq 1, the energy density is affected by both strain and modulus. While DB-20 has a larger strain and moderate modulus, so the energy density is relatively large. In addition, the energy density of DB-20 is 0.12 J/cm^3 at 150 MV/m because of its big modulus. Therefore, it is more favorable to be used as a relaxation ferroelectric for an artificial bone application.

As reported by us previously,[23] using eq 2, the strain of relaxor ferroelectrics can be divided into Maxwell stress-induced strain (S_M) from the amorphous phase and electrostriction strain (S_E) from the ferroelectric phase and relaxor ferroelectric phase,

$$S_3 = S_M + S_E \tag{2}$$

$$S_M = -0.5PE(1 + 2\nu)/Y \tag{3}$$

$$S_E = Q'P'^2 \tag{4}$$

where S_3, S_M, S_E, P, E, and Y are the strain, the strain derived from Maxwell stress, the strain from electrostriction, the polarization, the electric field, and the Young's modulus, respectively. In addition, ν is Poisson's ratio about 0.24−0.30, Q' is the electrostrictive coefficient, and P' represents polarization involving dipoles in the polar ferroelectric phase and relaxor ferroelectric phase. Because Y of normal ferroelectric polymers is large, they possess small S_M, and their S_3 is close to S_E. However, due to the low crystallinity of the relaxor ferroelectric polymer, S_M is too large to be ignored.

The strains of P(VDF-TrFE-DB)s and P(VDF-TrFE) are divided into S_M and S_E by theoretical simulation as shown in eqs 3 and 4 in order to study the relationship between strain and crystal phase carefully. Figure 8 shows the strains as a function of electric field from the contribution of Maxwell stress and induced electrostriction. In P(VDF-TrFE-DB)s, the proportion of S_E is basically zero under low electric field, and it starts to increase and then reaches equilibrium when the electric field increases to 30 MV/m. From eq 3, it can be seen that S_M is proportional to the dielectric constant and inversely proportional to the modulus, and S_E is related to the number of dipole orientations under the electric field. The dipole of P(VDF-TrFE-DB) cannot be oriented under a low electric field, so the percentage of S_E is very low. When the electric field increases to around 30 MV/m, S_E begins to increase because many of the dipoles start to orient. When the electric field further increases, the dipole orientation tends to be saturated, so the percentage of S_E reaches equilibrium. Namely, S_E appears like the start-up electric field under the low electric field. In addition, as the DB content increases, both the crystallinity and modulus decrease, and the dipole orientation-required electric field decreases as well. As a result, the start-up electric field decreases, and the proportion of S_E decreases at the final equilibrium, which is consistent with the previous analysis.

TrFE-20 has the highest S_E start-up electric field of 90 MV/m, which is about three times that of DB-20 (about 30 MV/m). S_E of TrFE mainly comes from the orientation of dipoles, associating with the E_c. Therefore, the proportion of S_E in TrFE-20 is about 75%, while that of DB-20 is only about 33% when the final balance is reached. The ferroelectric phase content plays the dominant role as discussed above.

CONCLUSIONS

By hydrogenation and elimination reaction of pristine P(VDF-CTFE)(65/35 mol %), a range of P(VDF-TrFE-DB) materials with different compositions are synthesized in order to study the effect of DB on the ferroelectric and electroactive properties of P(VDF-TrFE). DB could change the crystalline and ferroelectric phases of P(VDF-TrFE) and thus the dielectric, ferroelectric, and electroactive performances. A small amount of G conformation into the long-range ordered TTTT conformation appeared after the introduction of DB, thereby increasing the molecular chain spacing and transforming the ferroelectric phase copolymer into a relaxor ferroelectric phase. In addition, the reduction of T_C, the frequency dependence of the Curie phase transition peak, and the relaxation characteristics of the $D-E$ loop further confirmed the transformation of P(VDF-TrFE) from ferroelectrics to relaxor ferroelectrics because of the presence of DB. The lower polarization electric field and better electroactive performance of P(VDF-TrFE-DB) offer great electrostrain applications. This work skillfully uses the introduction of DBs to construct a relaxor ferroelectric polymer with a low driving electric field and a large electric strain, which provides a new strategy for the study of new ferroelectric polymer materials.

ASSOCIATED CONTENT

Supporting Information

The Supporting Information is available free of charge at https://pubs.acs.org/doi/10.1021/acsomega.2c05172.

DSC curve of P(VDF-TrFE) and P(VDF-TrFE-CTFE)-s; detailed calculation results of DSC and XRD; ε'' dependence on the temperature; d_{33} of P(VDF-TrFE-DB)s and P(VDF-TrFE) polymers; and strain (S_3) and the volumetric elastic energy density of P(VDF-TrFE) at 10 Hz (PDF)

https://doi.org/10.1021/acsomega.2c05172
ACS Omega 2022, 7, 42949−42959

AUTHOR INFORMATION

Corresponding Author

Zhicheng Zhang − *Xi'an Key Laboratory of Sustainable Energy Materials Chemistry, Department of Applied Chemistry, School of Chemistry, Xi'an Jiaotong University, Xi'an 710049 Shaanxi Province, P. R. China;* orcid.org/0000-0003-1871-117X; Email: zhichengzhang@mail.xjtu.edu.cn

Authors

Honghong Gong − *Xi'an Key Laboratory of Sustainable Energy Materials Chemistry, Department of Applied Chemistry, School of Chemistry, Xi'an Jiaotong University, Xi'an 710049 Shaanxi Province, P. R. China; Xi'an Jiaotong University Suzhou Academy, Suzhou 215123 Jiangsu Province, P. R. China*

Xiao Wang − *Xi'an Key Laboratory of Sustainable Energy Materials Chemistry, Department of Applied Chemistry, School of Chemistry, Xi'an Jiaotong University, Xi'an 710049 Shaanxi Province, P. R. China*

Mengdi Sun − *Xi'an Key Laboratory of Sustainable Energy Materials Chemistry, Department of Applied Chemistry, School of Chemistry, Xi'an Jiaotong University, Xi'an 710049 Shaanxi Province, P. R. China*

Ying Zhang − *Xi'an Key Laboratory of Sustainable Energy Materials Chemistry, Department of Applied Chemistry, School of Chemistry, Xi'an Jiaotong University, Xi'an 710049 Shaanxi Province, P. R. China*

Qinglong Ji − *Xi'an Key Laboratory of Sustainable Energy Materials Chemistry, Department of Applied Chemistry, School of Chemistry, Xi'an Jiaotong University, Xi'an 710049 Shaanxi Province, P. R. China; Xi'an Jiaotong University Suzhou Academy, Suzhou 215123 Jiangsu Province, P. R. China*

Complete contact information is available at: https://pubs.acs.org/10.1021/acsomega.2c05172

Author Contributions

Honghong Gong: investigation, formal analysis, preparing and editing the manuscript. Xiao Wang: investigation, formal analysis. Mengdi Sun, Ying Zhang, and Qinglong Ji: reading and working on the scientific language of the manuscript. Zhicheng Zhang: supervision, writing-review and editing, and funding acquisition.

Notes

The authors declare no competing financial interest.

ACKNOWLEDGMENTS

This work was financially supported by the Major Research Plan of the National Natural Science Foundation of China (Grant No. 92066204), the National Natural Science Foundation of China (Grant Nos. 52003214, 52073225), China Postdoctoral Science Foundation Funded Project (2019M663699 and 2020T130507), Shaanxi Province Key Research and Development Program (2021GXLH-Z-019, 2019JM-030), Natural Science Foundation of Jiangsu Province (BK2020245), Suzhou Science and Technology Project (SYG202028), and the Fundamental Research Funds for the Central Universities (xzy012020035). The authors thank the Instrument Analysis Center of Xi'an Jiaotong University for the kind help during the measurement process.

REFERENCES

(1) Chen, D.; Pei, Q. Electronic Muscles and Skins: A Review of Soft Sensors and Actuators. *Chem. Rev.* **2017**, *117*, 11239−11268.

(2) Zhang, Y.; Ellingford, C.; Zhang, R.; Roscow, J.; Hopkins, M.; Keogh, P.; McNally, T.; Bowen, C.; Wan, C. Electrical and Mechanical Self-Healing in High-Performance Dielectric Elastomer Actuator Materials. *Adv. Funct. Mater.* **2019**, *29*, 1808431.

(3) Yin, L. J.; Zhao, Y.; Zhu, J.; Yang, M.; Zhao, H.; Pei, J. Y.; Zhong, S. L.; Dang, Z. M. Soft, tough, and fast polyacrylate dielectric elastomer for non-magnetic motor. *Nat. Commun.* **2021**, *12*, 4517.

(4) Gai, Y.; Li, H.; Li, Z. Self-Healing Functional Electronic Devices. *Small* **2021**, *17*, e2101383.

(5) Keplinger, C.; Sun, J.-Y.; Foo, C. C.; Rothemund, P.; Whitesides, G. M.; Suo, Z. Stretchable, Transparent, Ionic Conductors. *Science* **2013**, *341*, 984−987.

(6) Ren, Z.; Kim, S.; Ji, X.; Zhu, W.; Niroui, F.; Kong, J.; Chen, Y. A High-Lift Micro-Aerial-Robot Powered by Low-Voltage and Long-Endurance Dielectric Elastomer Actuators. *Adv. Mater.* **2022**, *34*, e2106757.

(7) Martins, P.; Correia, D. M.; Correia, V.; Lanceros-Mendez, S. Polymer-based actuators: back to the future. *Phys. Chem. Chem. Phys.* **2020**, *22*, 15163−15182.

(8) Sheima, Y.; Caspari, P.; Opris, D. M. Artificial Muscles: Dielectric Elastomers Responsive to Low Voltages. *Macromol. Rapid Commun.* **2019**, *40* (16), e1900205.

(9) Cen, Z.; Huan, Y.; Feng, W.; Yu, Y.; Zhao, P.; Chen, L.; Zhu, C.; Li, L.; Wang, X. A high temperature stable piezoelectric strain of KNN-based ceramics. *J. Mater. Chem. A* **2018**, *6*, 19967−19973.

(10) Wu, B.; Ma, J.; Wu, W.; Chen, M. Improved piezoelectricity in ternary potassium-sodium niobate lead-free ceramics with large strain. *J. Mater. Chem. C* **2020**, *8*, 2838−2846.

(11) Yuan, H.; Li, L.; Hong, H.; Ying, Z.; Zheng, X.; Zhang, L.; Wen, F.; Xu, Z.; Wu, W.; Wang, G. Low sintering temperature, large strain and reduced strain hysteresis of $BiFeO_3$-$BaTiO_3$ ceramics for piezoelectric multilayer actuator applications. *Ceram. Int.* **2021**, *47*, 31349−31356.

(12) Chang, Y.; Wu, J.; Yang, B.; Xie, H.; Yang, S.; Sun, Y.; Zhang, S.; Li, F.; Cao, W. Large, thermally stabilized and fatigue-resistant piezoelectric strain response in textured relaxor-$PbTiO_3$ ferroelectric ceramics. *J. Mater. Chem. C* **2021**, *9*, 2008−2015.

(13) Hou, L.; Zhou, C.; Li, Q.; Li, R.; Yuan, C.; Xu, J.; Rao, G. Giant strain with ultra-low hysteresis by tailoring relaxor temperature and PNRs dynamic in BNT-based lead-free piezoelectric ceramics. *Ceram. Int.* **2022**, *48*, 13125−13133.

(14) Qiu, Y.; Zhang, E.; Plamthottam, R.; Pei, Q. Dielectric Elastomer Artificial Muscle: Materials Innovations and Device Explorations. *Acc. Chem. Res.* **2019**, *52*, 316−325.

(15) Li, Q.; He, Y.; Tan, S.; Zhu, B.; Zhang, X.; Zhang, Z. Dielectric elastomer with excellent electromechanical performance by dipole manipulation of Poly(vinyl chloride) for artificial muscles under low driving voltage application. *Chem. Eng. J.* **2022**, *441*, 136000.

(16) Yang, T.; Liu, L.; Li, X.; Zhang, L. High performance silicate/silicone elastomer dielectric composites. *Polymer* **2022**, *240*, 124470.

(17) Ellingford, C.; Zhang, R.; Wemyss, A. M.; Bowen, C.; McNally, T.; Figiel, L.; Wan, C. Intrinsic Tuning of Poly(styrene-butadiene-styrene)-Based Self-Healing Dielectric Elastomer Actuators with Enhanced Electromechanical Properties. *ACS Appl. Mater. Interfaces* **2018**, *10*, 38438−38448.

(18) Ellingford, C.; Zhang, R.; Wemyss, A. M.; Zhang, Y.; Brown, O. B.; Zhou, H.; Keogh, P.; Bowen, C.; Wan, C. Self-Healing Dielectric Elastomers for Damage-Tolerant Actuation and Energy Harvesting. *ACS Appl. Mater. Interfaces* **2020**, *12*, 7595−7604.

(19) Engel, K. E.; Kilmartin, P. A.; Diegel, O. Recent advances in the 3D printing of ionic electroactive polymers and core ionomeric materials. *Polym. Chem.* **2022**, *13*, 456−473.

(20) Lu, S. G.; Chen, X.; Levard, T.; Diglio, P. J.; Gorny, L. J.; Rahn, C. D.; Zhang, Q. M. Large Displacement in Relaxor Ferroelectric Terpolymer Blend Derived Actuators Using Al Electrode for Braille Displays. *Sci. Rep.* **2015**, *5*, 11361.

(21) Zhu, Z.; Rui, G.; Li, Q.; Allahyarov, E.; Li, R.; Soulestin, T.; Domingues Dos Santos, F.; He, H.; Taylor, P. L.; Zhu, L. Electrostriction-enhanced giant piezoelectricity via relaxor-like secondary crystals in extended-chain ferroelectric polymers. *Matter* **2021**, *4*, 3696−3709.
(22) Zhang, Z.; Wang, X.; Tan, S.; Wang, Q. Superior electrostrictive strain achieved under low electric fields in relaxor ferroelectric polymers. *J. Mater. Chem. A* **2019**, *7*, 5201−5208.
(23) Qiao, B.; Wang, X.; Tan, S.; Zhu, W.; Zhang, Z. Synergistic Effects of Maxwell Stress and Electrostriction in Electromechanical Properties of Poly(vinylidene fluoride)-Based Ferroelectric Polymers. *Macromolecules* **2019**, *52*, 9000−9011.
(24) Wang, X.; Qiao, B.; Tan, S.; Zhu, W.; Zhang, Z. Tuning the ferroelectric phase transition of PVDF by uniaxially stretching crosslinked PVDF films with CF═CH bonds. *J. Mater. Chem. C* **2020**, *8*, 11426−11440.
(25) Huang, Y.; Xu, J.-Z.; Soulestin, T.; Dos Santos, F. D.; Li, R.; Fukuto, M.; Lei, J.; Zhong, G.-J.; Li, Z.-M.; Li, Y.; Zhu, L. Can Relaxor Ferroelectric Behavior Be Realized for Poly(vinylidene fluoride-*co*-chlorotrifluoroethylene) [P(VDF-CTFE)] Random Copolymers by Inclusion of CTFE Units in PVDF Crystals? *Macromolecules* **2018**, *51*, 5460−5472.
(26) Liu, Y.; Aziguli, H.; Zhang, B.; Xu, W.; Lu, W.; Bernholc, J.; Wang, Q. Ferroelectric polymers exhibiting behaviour reminiscent of a morphotropic phase boundary. *Nature* **2018**, *562*, 96−100.
(27) Wongwirat, T.; Zhu, Z.; Rui, G.; Li, R.; Laoratanakul, P.; He, H.; Manuspiya, H.; Zhu, L. Origins of Electrostriction in Poly(vinylidene fluoride)-Based Ferroelectric Polymers. *Macromolecules* **2020**, *53*, 10942−10954.
(28) Zhu, Z.; Rui, G.; Li, R.; He, H.; Zhu, L. Enhancing Electrostrictive Actuation via Strong Electrostatic Repulsion among Field-Induced Nanodomains in a Relaxor Ferroelectric Poly(vinylidene fluoride-*co*-trifluoroethylene-*co*-chlorotrifluoroethylene) Random Terpolymer. *ACS Appl. Mater. Interfaces* **2021**, *13*, 42063−42073.
(29) Liu, Z.; Li, S.; Zhu, J.; Mi, L.; Zheng, G. Fabrication of *β*-Phase-Enriched PVDF Sheets for Self-Powered Piezoelectric Sensing. *ACS Appl. Mater. Interfaces* **2022**, *14*, 11854−11863.
(30) Li, Z.; Liao, J.; Xi, Z.; Zhu, W.; Zhang, Z. Influence of Steric Hindrance on Ferro- and Piezoelectric Performance of Poly(vinylidene fluoride)-Based Ferroelectric Polymers. *Macromol. Chem. Phys.* **2019**, *220*, 1900273.
(31) Lu, L.; Ding, W.; Liu, J.; Yang, B. Flexible PVDF based piezoelectric nanogenerators. *Nano Energy* **2020**, *78*, 105251.
(32) Chen, X.; Qin, H.; Qian, X.; Zhu, W.; Li, B.; Zhang, B.; Lu, W.; Li, R.; Zhang, S.; Zhu, L.; Santos, F. D. D.; Bernholc, J.; Zhang, Q. M. Relaxor ferroelectric polymer exhibits ultrahigh electromechanical coupling at low electric field. *Science* **2022**, *375*, 1418−1422.
(33) Soulestin, T.; Ladmiral, V.; Dos Santos, F. D.; Améduri, B. Vinylidene fluoride- and trifluoroethylene-containing fluorinated electroactive copolymers. How does chemistry impact properties? *Prog. Polym. Sci.* **2017**, *72*, 16−60.
(34) Li, M.; Wondergem, H. J.; Spijkman, M. J.; Asadi, K.; Katsouras, I.; Blom, P. W.; de Leeuw, D. M. Revisiting the delta-phase of poly(vinylidene fluoride) for solution-processed ferroelectric thin films. *Nat. Mater.* **2013**, *12*, 433−438.
(35) Lheritier, P.; Vaxelaire, N.; Tencé-Girault, S.; Domingues Dos Santos, F.; Defay, E. Influence of field-induced phase transition on poly(vinylidene fluoride-trifluorethylene-chlorotrifluoroethylene) strain. *Phys. Rev. Appl.* **2020**, *14*, 044061.
(36) Cheng Huang; Klein, R.; Feng Xia; Hengfeng Li; Zhang, Q.M.; Bauer, F.; Cheng, Z.-Y. Poly(vinylidene fluoride-trifluoroethylene) based high performance electroactive polymers. *IEEE Trans. Dielectr. Electr. Insul.* **2004**, *11*, 299−311.
(37) Zhang, Q. M.; Li, H.; Poh, M.; Xia, F.; Cheng, Z. Y.; Xu, H.; Huang, C. An all-organic composite actuator material with a high dielectric constant. *Nature* **2002**, *419*, 284−287.
(38) Zhang, Q. M.; Bharti, V.; Zhao, X. Giant Electrostriction and Relaxor Ferroelectric Behavior in Electron-Irradiated Poly(vinylidene fluoride-trifluoroethylene) Copolymer. *Science* **1998**, *280*, 2101−2104.
(39) Yang, L.; Tyburski, B. A.; Dos Santos, F. D.; Endoh, M. K.; Koga, T.; Huang, D.; Wang, Y.; Zhu, L. Relaxor Ferroelectric Behavior from Strong Physical Pinning in a Poly(vinylidene fluoride-*co*-trifluoroethylene-*co*-chlorotrifluoroethylene) Random Terpolymer. *Macromolecules* **2014**, *47*, 8119−8125.
(40) Zhang, M.; Tan, S.; Xiong, J.; Chen, C.; Zhang, Y.; Wei, X.; Zhang, Z. Tailoring Dielectric and Energy Storage Performance of PVDF-Based Relaxor Ferroelectrics with Hydrogen Bonds. *ACS Appl. Energy Mater.* **2021**, *4*, 8454−8464.
(41) Li, J.; Hu, X.; Gao, G.; Ding, S.; Li, H.; Yang, L.; Zhang, Z. Tuning phase transition and ferroelectric properties of poly(vinylidene fluoride-*co*-trifluoroethylene) via grafting with desired poly(methacrylic ester)s as side chains. *J. Mater. Chem. C* **2013**, *1*, 1111−1121.
(42) Cheng, Z.; Zhang, Q. Field-Activated Electroactive Polymers. *MRS Bull.* **2008**, *33*, 183−187.
(43) Lu, Y.; Claude, J.; Neese, B.; Zhang, Q.; Wang, Q. A Modular Approach to Ferroelectric Polymers with Chemically Tunable Curie Temperatures and Dielectric Constants. *J. Am. Chem. Soc.* **2006**, *128*, 8120−8121.
(44) Zhang, Z.; Chung, T. C. M. The Structure-Property Relationship of Poly(vinylidene difluoride)-Based Polymers with Energy Storage and Loss under Applied Electric Fields. *Macromolecules* **2007**, *40*, 9391−9397.
(45) Xu, H.; Cheng, Z.-Y.; Olson, D.; Mai, T.; Zhang, Q. M.; Kavarnos, G. Ferroelectric and electromechanical properties of poly(vinylidene fluoride-trifluoroethylene chlorotrifluoroethylene) terpolymer. *Appl. Phys. Lett.* **2001**, *78*, 2360−2362.
(46) Li, J.; Tan, S.; Ding, S.; Li, H.; Yang, L.; Zhang, Z. High-field antiferroelectric behaviour and minimized energy loss in poly(vinylidene-*co*-trifluoroethylene)-*graft*-poly(ethyl methacrylate) for energy storage application. *J. Mater. Chem.* **2012**, *22*, 23468−23476.
(47) Liu, J.; Zhao, Y.; Chen, C.; Wei, X.; Zhang, Z. Study on the Polarization and Relaxation Processes of Ferroelectric Polymer Films Using the Sawyer-Tower Circuit with Square Voltage Waveform. *J. Phys. Chem. C* **2017**, *12*, 12531−12539.

https://doi.org/10.1021/acsomega.2c05172
ACS Omega 2022, 7, 42949−42959